Simulations of multi-beam sonar echos from schooling individual fish in a quiet environment

Arne Johannes Holmin[a)]
Department of Mathematics, University of Bergen, P.O. Box 7800, 5020 Bergen, Norway

Nils Olav Handegard and Rolf J. Korneliussen
Institute of Marine Research, P.O. Box 1870 Nordnes, 5817 Bergen, Norway

Dag Tjøstheim
Department of Mathematics, University of Bergen, P.O. Box 7800, 5020 Bergen, Norway

(Received 23 March 2012; revised 12 September 2012; accepted 2 October 2012)

A model is developed and demonstrated for simulating echosounder and sonar observations of fish schools with specified shapes and composed of individuals having specified target strengths and behaviors. The model emulates the performances of actual multi-frequency echosounders and multi-beam echosounders and sonars and generates synthetic echograms of fish schools that can be compared with real echograms. The model enables acoustic observations of large *in situ* fish schools to be evaluated in terms of individual and aggregated fish behaviors. It also facilitates analyses of the sensitivity of fish biomass estimates to different target strength models and their parameterizations. To demonstrate how this tool may facilitate objective interpretations of acoustically estimated fish biomass and behavior, simulated echograms of fish with different spatial and orientation distributions are compared with real echograms of herring collected with a multi-beam sonar aboard the research vessel "G.O. Sars." Results highlight the important effects of fish-backscatter directivity, particularly when sensing with small acoustic wavelengths relative to the fish length. Results also show that directivity is both a potential obstacle to estimating fish biomass accurately and a potential source of information about fish behavior.
 [http://dx.doi.org/10.1121/1.4763981]

PACS number(s): 43.30.Sf, 43.30.Ft, 43.60.Cg [AMT] Pages: 3720–3734

I. INTRODUCTION

Acoustic measurements of marine life span spatial scales ranging from millimeters[1] to thousands of meters,[2] and contemporary sonar equipment (e.g., Simrad MS70) can provide observations of large *in situ* fish aggregations, synoptically, with high spatiotemporal resolution. However, whereas acoustic instruments have become increasingly sophisticated, interpretation of their data is still a major challenge. For example, when measurements are made with a multi-beam echosounder (MBE; projecting mostly downward) or multi-beam sonar (MBS; projecting mostly laterally)[3] versus a conventional single-beam echosounder (SBE; projecting vertically downward), it is more important to consider the dependence of backscatter (i.e., echo energy in the direction of the sensing transducer) on acoustic frequency and incidence angle.

A. Backscattering directivity

For a monostatic sonar, which has co-located transmitter and receiver, directivity describes the dependence of backscatter on the angle between the incident acoustic wave and a target. Backscattering directivity, a function of acoustic frequency, may cause measurements of integrated backscatter[4,5] to vary greatly, particularly when the acoustic wavelength is small relative to the target size. Unfortunately target orientations relative to the sound beam(s) depend on animal behavior, which is generally unknown. On the other hand, variations in echoes may provide useful information about school dynamics,[6] such as synchronized changes in fish orientation in response to a predator.[7]

B. Target strength models

The effects of backscattering directivity on sonar observations of fish have been investigated by numerous researchers for several decades. Intrinsically, these investigations involve estimates of fish target strength (TS). TS is a metric of an object's reflectivity, which is dependent on the acoustic frequency[8] and incidence angle,[9] and the animal's size, morphology, and physiology.[10] Love[9] pioneered the measurement and modeling of fish backscatter from any incidence angle. Subsequently, numerous others have investigated the scattering directivity of fish and other marine organisms, e.g., herring[11] and krill.[12,13] McClatchie and Ye[14] used simple geometries like a prolate spheroid[15] and a deformed cylinder[16] to approximate the scattering directivity of fish with swim bladders.

Perhaps the most commonly used model for fish TS is the Kirchhoff ray-mode (KRM) model.[17] The KRM model represents a target's shape by a collection of simple geometric objects, and TS is calculated as the coherent addition of their echoes. With correct parameter values, the KRM model performs well for oblong targets at angles close to normal

a)Author to whom correspondence should be addressed. Electronic mail: Arne.Holmin@math.uib.no

incidence.[17] However, the model is inaccurate at large angles of incidence where it generally underestimates the backscatter.[18] Because the use of sonars has increased, so has the need for accurate models of TS versus acoustic frequency and all incidence angles. As an alternative to the KRM model, the Fourier matching method considers axisymmetric objects of irregular shape and should be unbiased at all aspects (Reeder *et al.*[18]).

C. Simulation models

Models of fish TS have been used to simulate data from real echosounders and sonars. Analyses of simulated data, often in comparison to real data, have provided knowledge about the validities of the TS models, characteristics of the targets, performances of the instruments, and the qualities of echo-integration analyses. The accuracy of simulated data depends greatly, however, on the accuracies of the TS and sonar-performance models and their parameterizations and the extent to which other important factors, e.g., noise, are considered.

Foote[19] developed a simulation model for an SBE to validate an echo-integration method.[20] He modeled the acoustic beam resulting from a circular piston transducer, fish TS with an empirical backscattering directivity function,[21] and the resulting echo signal with incoherently added noise. Coombs and Barr[22] developed a model to simulate echoes from fish received with an SBE. They estimated the normal distributions of the swim bladder tilt angle of black and smooth oreos based on a least squares criterion of the difference between *in situ* TS measurements and simulated TS measurements of KRM models for a variety of tilt angle distributions. Diner[23] simulated echograms from an SBE to quantify and correct for the distortion of school metrics resulting from the acoustic beam width. Demer *et al.*[24] developed a simulation model for a multi-frequency SBE and used it to verify the performance of a method for better rejecting echoes from non-resolvable coincident targets. Horne and Jech[25] estimated fish length distributions by inverting a KRM model of fish TS using multi-frequency measurements of fish TS.

Buelens *et al.*[26] developed a model of an MBE that incorporated beam forming, sound-ray tracing, and target scattering to simulate received acoustic intensities. They used the data to develop methods for target classification. Cutter and Demer[27] used a KRM model of fish TS and simulated MBE observations of fish schools exhibiting a variety of behaviors, e.g., diving close to the vessel. They recognized the simulated patterns in real MBE measurements, illustrating the usefulness of such simulations. The effects of scattering directivity on measurements from an SBE (vertically oriented) and a sonar (horizontally oriented) were further demonstrated through simulations by Henderson *et al.*[28] and Boswell *et al.*,[5] respectively. The latter group noted high variability in biomass estimates due to changes in mean orientation for polarized groups of fish.

D. Scattering statistics

Scattering variability may also arise from constructive and destructive interference of waves reflecting from multiple fish within a school. According to Stanton,[29] the amplitude A of the sum of a sufficient number of sine waves of uniformly distributed phase is approximately Rayleigh distributed with probability density function (PDF)

$$f_A(x) = \frac{x}{\sigma^2} e^{-x^2/2\sigma^2}, \tag{1}$$

with parameter $\sigma^2 = \sum_l a_l^2/2$, where a_l is the amplitude of the lth sine wave. It can be shown that Rayleigh distributed pressure amplitude implies exponentially distributed intensity I with mean equal to the sum of the individual intensities. Considering the univariate transformation $A = \sqrt{2\lambda\sigma^2 I}$ for an arbitrary constant $\lambda > 0$, with Jacobian $|\mathrm{d}A/\mathrm{d}I| = |\lambda\sigma^2/\sqrt{2\lambda\sigma^2 I}|$, the PDF of I follows from the Rayleigh distribution given in Eq. (1):

$$f_I(x) = \frac{\sqrt{2\lambda\sigma^2 x}}{\sigma^2} \exp\left(\frac{-2\lambda\sigma^2 x}{2\sigma^2}\right) \left|\frac{\lambda\sigma^2}{\sqrt{2\lambda\sigma^2 x}}\right| = \lambda e^{-\lambda x}, \tag{2}$$

where the expectation of I can be expressed as $\mathrm{E}(I) = \lambda^{-1} = \sum_l I_l$ by applying the relation $I = A^2/2\rho_0 c$ to the transformation, resulting in $\lambda^{-1} = \sigma^2/\rho_0 c = \sum_l a_l^2/2\rho_0 c$, where $\rho_0 c$ is the specific acoustic impedance of a plane wave.

When few targets contribute to the echo received in a specific sampling interval, Chu and Stanton[30] note that the pressure amplitude is not well approximated by the Rayleigh distribution. This non-Rayleigh property is most evident if the number of targets scattering sound of similar pressure amplitude is less than five [plots for 2, 3, 4, and 100 identical amplitudes are given in Chu and Stanton,[30] their Fig. 2]. The exact PDFs of the pressure amplitude and the corresponding intensity from a finite number of targets of known, and possibly unequal individual pressure amplitudes was calculated by Barakat[31] (his Eqs. 31, 55, 56, and 64). See Sec. II B 2 for implementation of the PDF of the intensity in the simulation model.

E. Study objectives

In this study, we develop and demonstrate a model that accepts input that includes: The properties of an SBE, MBE, or MBS, and the propagation media; and the number, positions, and orientations of targets comprising an aggregation. It outputs simulated data for the specified instrument. The model facilitates the interpretation of real multi-beam data in terms of individual fish behaviors[32] and their aggregation morphology[33,34] and dynamics.[35] Furthermore, hypotheses regarding the spatiotemporal and orientational distributions of the targets[36] comprising a school, and their aggregate behavior, can be translated by the model to simulated acoustic observations for comparisons to real data.

The objectives of this study are to (1) develop a software tool, based on theoretical backscatter from individual fish, to predict acoustic backscatter from fish schools; (2) adapt the tool to simulate output from standard instruments used to survey and study fish; and (3) demonstrate how the simulation tool can be used to interpret real acoustic data in studies of fish behavior and aggregation characteristics.

II. MATERIALS AND METHODS

A. Simulation model

A model is developed that simulates echoes from fish schools, and measurements of TS and volume backscattering strength (S_v) made with an SBE (i.e., Simrad EK60), MBE (i.e., Simrad ME70), or MBS (i.e., Simrad MS70) in an environment with no background noise and no reverberation. The simulator incorporates models of fish TS, individual and aggregated fish behaviors, and measurement instrument performance. In this section, these models and their collective use to simulate data from the following scenarios are described: (1) single-beam observations of a single-target, (2) multi-beam observations of multiple targets, and (3) multi-beam observations of a standard sphere (calibration).

1. Coordinate systems

The simulated echosounder or sonar transducer is assumed to be monostatic. The transducer and targets are positioned in a global right-hand Cartesian coordinate system where the origin is located on the sea surface at a reference position of the research vessel, west is along the x axis; north is along the y axis, and vertically upward is along the z axis. Separate right-hand Cartesian coordinate systems are defined for the transducer beams and for the targets (Fig. 1). Both of these coordinate systems differ from the global coordinate system by having z axis oriented along the direction of the beam/target, represented by the maximum response in the case of a beam and the heading in the case of a target as opposed to vertically upward. This definition has the advantage that in the corresponding spherical coordinate systems, the elevation angle of a position vector is defined as the angle between the position vector and the direction of the beam/target. In the case of a transducer beam, the origin is located on the transducer face; the direction of the beam is along the z axis; the sea surface is parallel to the x axis; and vertically downward is positive on the y axis for non-vertical beams. For beams pointing vertically downward, the negative vessel direction is along the y axis, and for beams pointing vertically upward, the positive vessel direction is along the y axis. Similarly, for a target, the origin is the center of mass; the direction of the target is along the positive z axis; the sea surface is parallel to the x axis; and vertically downward is positive on the y axis (i.e., down through the abdomen of a fish).

To represent the position of a target by its range and incidence angle to a beam and, similarly, to represent the position of the transducer by its range and incidence angle to a target, spherical coordinate systems are defined for the transducer beams and the targets. In the spherical coordinate system of a transducer beam, the position of the target (r, θ, ϕ), is defined by the range r, the azimuth angle θ, and the elevation angle ϕ. The corresponding notation for the position of the transducer in the spherical coordinate system of the target is (r', θ', ϕ'). During the period between transmission and reception, the movement of a vessel-mounted transducer is assumed to be small enough that the change in r is negligible $(r' \approx r)$. Sound speed c is assumed to be constant throughout the propagation path, so refraction is not considered.

In the case of multiple beams aiming in different directions, there is a need for a definition of the right-hand Cartesian coordinate system of the research vessel. The origin of this coordinate system is located on the transducer face; starboard is along the x axis; vessel heading is along the y axis; and vertically upward (parallel to the mast) is along the z axis. The corresponding spherical coordinate system is defined by the range $r^\star$, the azimuth angle $\theta^\star$, and the elevation angle $\phi^\star$.

Transformation between the coordinate systems is done by the following method: Consider two coordinate systems, say C_1 and C_2, where the origin of C_2 is represented by o_2 in C_1, and where C_2 is rotated by the Euler angles τ_z, τ_x, and τ_y counter-clockwise around the z axis, x axis, and y axis of C_1, respectively. The transformation of a position vector v_1 in C_1 into the corresponding position vector v_2 in C_2 is obtained by subtraction of o_2 from v_1, followed by multiplication of the resulting vector by a rotation matrix $\mathbb{A}_{z,x,y}(\tau_z, \tau_x, \tau_y)$:

$$v_2 = \mathbb{A}_{z,x,y}(\tau_z, \tau_x, \tau_y)[v_1 - o_2]. \tag{3}$$

The rotation matrix is constructed by multiplication of single rotation matrices, $\mathbb{A}_{z,x,y}(\tau_z, \tau_x, \tau_y) = \mathbb{A}_y(\tau_y)\mathbb{A}_x(\tau_x)\mathbb{A}_z(\tau_z)$, where the single rotation matrices $\mathbb{A}_x(\tau_x)$, $\mathbb{A}_y(\tau_y)$, and $\mathbb{A}_z(\tau_z)$ represent counter-clockwise rotation around the x axis, y axis, and z axis, respectively, and are given by

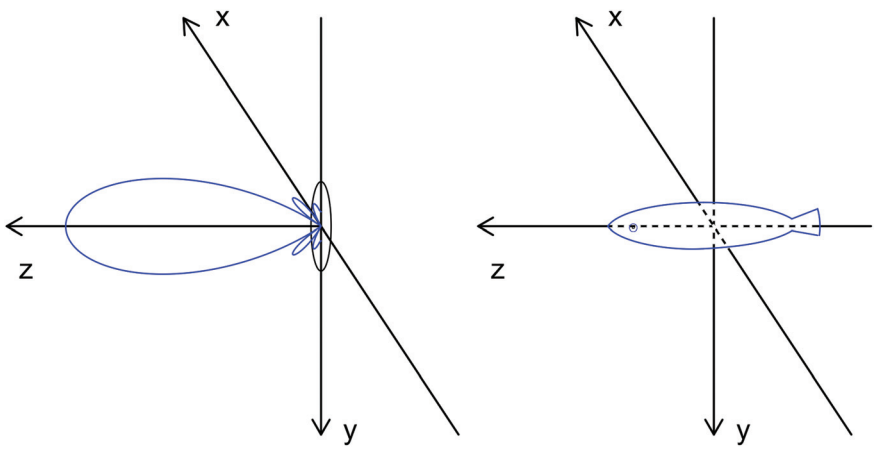

FIG. 1. Coordinate system of the transducer (left), and the target (right), represented in this case by a single fish.

$$\mathbb{A}_x(\tau_x) = \begin{bmatrix} 1 & 0 & 0 \\ 0 & \cos\tau_x & \sin\tau_x \\ 0 & -\sin\tau_x & \cos\tau_x \end{bmatrix},$$
$$\mathbb{A}_y(\tau_y) = \begin{bmatrix} \cos\tau_y & 0 & -\sin\tau_y \\ 0 & 1 & 0 \\ \sin\tau_y & 0 & \cos\tau_y \end{bmatrix},$$
$$\mathbb{A}_z(\tau_z) = \begin{bmatrix} \cos\tau_z & \sin\tau_z & 0 \\ -\sin\tau_z & \cos\tau_z & 0 \\ 0 & 0 & 1 \end{bmatrix}. \quad (4)$$

The rotation order z-x-y specified by the Euler angles corresponds to the yaw, pitch, and roll of C_2 relative to C_1, but arbitrary rotations can be constructed by multiplication of the single rotation matrices given in Eq. (4). Consider, for example, the transformation of the position vector v_G of a target in the global coordinate system C_G into the position vector v_B of the target in the coordinate system of a beam C_B. Denote the origin of C_B in C_G by o_B and define the rotation angles $\tau_{z,\mathrm{V}}$, $\tau_{x,\mathrm{V}}$, and $\tau_{y,\mathrm{V}}$, representing the yaw, pitch, and roll of the research vessel relative to C_G, respectively. The position vector v_B is given by $v_B = \mathbb{A}_x(-\phi^\star)\mathbb{A}_z(\theta^\star - \pi/2)\mathbb{A}_{z,x,y}(\tau_{z,\mathrm{V}}, \tau_{x,\mathrm{V}}, \tau_{y,\mathrm{V}})[v_G - o_B]$, where the translation $v_G - o_B$ centers the coordinate systems around a mutual origin; the rotation matrix $\mathbb{A}_{z,x,y}(\tau_{z,\mathrm{V}}, \tau_{x,\mathrm{V}}, \tau_{y,\mathrm{V}})$ aligns the coordinate system of the vessel C_V with C_G; and the rotation matrices $\mathbb{A}_z(\theta^\star - \pi/2)$ and $\mathbb{A}_x(-\phi^\star)\mathbb{A}_z$ specify the azimuth and elevation angle of the direction of the beam in C_V, where the subtraction of $\pi/2$ from $\theta^\star$ and the minus sign in $-\phi^\star$ are consequences of the definition of C_B given in this section.

2. Measurements of backscatter

The maximum intensity of the transmitted beam I_0 is modified in the direction of the target (θ, ϕ) by the transmit beam pattern $B_{\mathrm{T1}}(\theta, \phi)$. Over the range r from the transducer to the target, the sound intensity is attenuated by spherical spreading r^{-2} and absorption $10^{-\alpha r/10}$, where α is the frequency-dependent absorption coefficient in units of $\mathrm{dB\,m^{-1}}$. The backscattering cross-sectional area σ_{bs} of a target reflects a portion of the incident energy, and TS is its decibel representation $\mathrm{TS} = 10\log_{10}(\sigma_{\mathrm{bs}})$. The reflected intensity is attenuated again by $10^{-\alpha r/10}r^{-2}$ and finally modified by the receive beam pattern $B_{\mathrm{T2}}(\theta, \phi)$. The sound intensity received by a sounder I_{rec} provides measures of TS and volume backscattering coefficient s_v (MacLennan *et al.*[37]):

$$\mathrm{TS} = 10\log_{10}\left(10^{\alpha r/5}r^4\frac{I_{\mathrm{rec}}}{I_0 B_{\mathrm{T1}}(\theta', \phi')B_{\mathrm{T2}}(\theta', \phi')}\right), \quad (5)$$

$$s_v = \frac{1}{V}\sum_V 10^{\alpha r/5}r^4\frac{I_{\mathrm{rec}}}{I_0 B_{\mathrm{T1}}(\theta', \phi')B_{\mathrm{T2}}(\theta', \phi')}, \quad (6)$$

where V is the volume over which backscattering cross-sectional areas are summed. The mean volume backscattering strength $S_v = 10\log_{10}(s_v)$ is frequently used in particular for visualization purposes.

For a single transceiver beam of sampling duration Δt, the volume V is enclosed by the equivalent beam angle[38]

$$\psi = \int_{\theta=0}^{2\pi}\int_{\phi=0}^{\pi/2} B_{\mathrm{T1}}(\theta, \phi)B_{\mathrm{T2}}(\theta, \phi)\sin(\phi)\mathrm{d}\phi\mathrm{d}\theta, \quad (7)$$

which can be interpreted as the solid angle inside which an idealized beam pattern is 1; and the distances $r_j - \Delta t/2$ and $r_j + \Delta t/2$, where $r_j = (j-1)\Delta t$ is the distance from which the entire sound pulse backscattered from a point target is received in the jth right-open sample interval $[(j-1)\Delta t, j\Delta t)$, $j = 1, \ldots, J$. The volume of a spherical cone of range r in terms of ψ is $\psi r^3/3$, and taking the difference between the volume of spherical cones of radius $r_j + \Delta t/2$ and $r_j - \Delta t/2$ results in the following expression for the volume V:

$$V = \frac{\psi}{3}\left((r_j + \Delta t/2)^3 - (r_j - \Delta t/2)^3\right). \quad (8)$$

3. Model of fish target strength

The backscattering cross-sectional area σ_{bs} is a measure of the backscatter intensity at 1 m from a target relative to the incident intensity. In the simulation model, it is expressed as $\sigma_{\mathrm{bs}}(\theta', \phi', d) = \sigma_0\eta_{\mathrm{C}}\eta_\Omega B_{\mathrm{L}}(\theta', \phi')$, where the maximum backscattering cross-sectional area σ_0 is dependent on the measurement frequency f, the target size S (defined as the total length), shape, and morphology. Further, in the case of fish with a swim bladder, hydrostatic swim bladder compression reduces the echo energy absorbed in the target by the factor[39]

$$\eta_{\mathrm{C}} = \left(1 + \frac{d}{10}\right)^{\gamma_L + \gamma_W}, \quad (9)$$

where $\gamma_L \le 0$ and $\gamma_W \le 0$ represent compression in swim bladder length and width respectively, and $d \ge 0$ is the depth of the target in meters. Finally, σ_{bs} is modified by the backscattering directivity of the target, composed of the frequency independent orientation factor $\eta_\Omega \in [0, 1]$, representing the acoustic cross-sectional receiving area at aspect $\Omega = (\theta', \phi')$ relative to the maximum acoustic cross-sectional receiving area at the given depth, and the frequency dependent target beam pattern $B_{\mathrm{L}}(\theta', \phi')$ in the direction of the transducer. The backscattering directivity is particularly important in the case of measurements with MBE or MBS, where targets are observed at a wide range of aspects. Parametric functions or empirical tables are used to define B_{T1}, B_{T2}, B_{L}, and η_Ω.

For frequency $f = 38\,\mathrm{kHz}$, Ona[39] estimated the depth-dependence of dorsal-incidence target strength of herring by the expression $\mathrm{TS} = 20\log_{10}S - 2.3\log_{10}(1 + d/10) - 65.4$, where S is measured in cm. In the simulation model, this equation is expressed as $\sigma_0(f_0)\eta_{\mathrm{C}} = S^m 10^{-6.54}\eta_{\mathrm{C}}$, where $f_0 = 38\,\mathrm{kHz}$, $\eta_{\mathrm{C}} = (1 + d/10)^{-0.23}$ and $m = 2$. It is assumed that swim bladder compression occurs only radially ($\gamma_{\mathrm{L}} = 0$ and $\gamma_{\mathrm{W}} = -0.23$). Therefore σ_{bs} decreases and the oblongness ξ, defined by the ratio between length and width of the swim bladder, increases with increasing depth.

The ratio $\sigma_0(f)/\sigma_0(f_0)$ was 1.37, 1.00, 0.85, 0.64, and 0.41 at frequencies 18, 38, 70, 120, and 200 kHz, respectively, in the results of five surveys of herring near Norway during

1996 to 2010 (unpublished data). Backscatter for 333 kHz was also available but was not estimated due to fewer reliable observations and higher variability at this frequency. The model $\sigma_0(f)/\sigma_0(f_0) = (f/f_0)^{\gamma_f}$ was fitted to these data by the least-squares method, resulting in the estimate $\gamma_f = -0.4$, rounded off to the nearest 0.1 because of the uncertainty of the data related to the extended period of observation, potentially including annual differences in size composition and other properties of the herring. This estimate results in $\sigma_0(f) = \epsilon_\sigma(f)S^2$, where $\epsilon_\sigma(f) = 10^{-6.54}\ (f/f_0)^{-0.4}$ is a species-specific, frequency dependent constant linking the maximum backscattering cross-sectional area to squared fish size. Fish sizes S were drawn from the Normal distribution N(mean = 32 cm, standard deviation = 2 cm).

In most of the simulations, the prolate-spheroid modal-series (PSMS) model[15] was used to estimate scatter from a vacant prolate spheroid with oblongness $\xi = 5$, representing the swim bladder. Scatter from the remainder of the fish body was ignored. The target beam pattern B_L was calculated as in Tang *et al.*[15] for a grid of incidence angles $\phi' = 0°, 0.5°, \ldots, 90°$, and $kL = 0.2, 1.2, \ldots, 47.2$, where $k = 2\pi f/c$ is the wave number, and $L = 0.26 \cdot S$ (Gorska and Ona[40]) is the long dimension of the prolate spheroid corresponding to swim bladder length. For values of $kL = 48.2, 49.2, \ldots, 300.2$, the method used by Tang did not perform satisfactorily, and estimates of the target beam pattern were calculated by use of the KRM model of a prolate spheroid despite its limited accuracy at large angles of incidence. For the frequencies used in the ME70 and the MS70, the majority of the fish had $kL \leq 47.2$, and the beam pattern estimates from the KRM, were thus only used for particularly large fish or at the higher frequencies of the EK60. In one of the simulations, for comparison to the prolate spheroid, a simple line-source model[1] was used. In that case, B_L was expressed by the sinc function of the product $kL\phi/2$, and the model used to calculate η_Ω was a cylinder rounded by hemispheres at both ends.

4. Model of fish behavior

In the examples presented in this paper, the individual fish trajectories were generated by the following model of fish behavior: At the initial time t_0, the positions of the individual fish are coordinates within a hypothetical fish school with specified density, shape, size, and initial position $\mathbf{x}_0$. The model of fish behavior assumes that the individual fish have a common underlying velocity component $\mathbf{v}_k$ at time t_k, $k \geq 0$, which can be manipulated to steer the expected center of mass of the school along a desired trajectory. The unperturbed position of the lth fish relative to the school position at time t_k is denoted by $\mathbf{y}_{l,k}$. Various behavior patterns, e.g., swarming, torus, or parallel alignment, may be simulated by including forced motion in $\mathbf{y}_{l,k}$. To include randomness in the orientation and position of each individual fish, an autoregressive perturbation $\mathbf{n}_{l,k}$ is added to the position of the lth fish at time t_k, given by

$$\mathbf{n}_{l,k} = \gamma \mathbf{n}_{l,k-1} + \varepsilon_{l,k}, \tag{10}$$

where the three component parameter γ satisfies $|\gamma| < 1$, and $\varepsilon_{l,k}$ has a Normal distribution with zero mean and three component vector of variances $\mathbf{v}$.

The position of the lth fish at the kth time step is then given by

$$\mathbf{X}_{l,k} = \mathbf{x}_0 + \sum_{i=1}^{k} \mathbf{v}_{i-1}(t_i - t_{i-1}) + \mathbf{y}_{l,k} + \mathbf{n}_{l,k}. \tag{11}$$

The model does not account for interactions between individuals other than through the underlying common velocity component $\mathbf{v}_k$. This is a simplification compared with other behavior models,[32] but the model serves as a fast way of generating the desired spatial and orientational characteristics of the fish schools.

In this study, parallel alignment was simulated by setting $\mathbf{y}_{l,k}$ equal to the position $\mathbf{y}_{l,0}$ at the initial time t_0, causing the position of each fish only to change by $\mathbf{n}_{l,k}$ relative to the school center. Also the school was given linear motion by setting $\mathbf{v}_k = \mathbf{v}_0$. The fish alignments are governed by $\mathbf{v}$, which was set to produce a desired polarization p, defined by the mean angle deviation between the headings of the individuals and the school.[36] The process was allowed to run for a number of 10 time steps before recording the trajectories so that the autoregressive process could reach a state unaffected by the initial positions.

B. Simulated scenarios

1. Single-beam observations of a single target

Consider an SBE insonifying a single target. Ignore the limited system bandwidth and acknowledge that dispersion of sound waves in water is negligible. For a sound pulse of duration equal to the sampling duration Δt, the acoustic intensity received by the SBE in the jth (right-open) sampling interval $[(j-1)\Delta t, j\Delta t)$, from a target at distance r, insonifying the receiver in the (right-open) time interval $[2r/c, 2r/c + \Delta t)$, is

$$I_{\mathrm{rec},j} = I_0 \frac{10^{-\alpha r/5}}{r^4} B_{T1}(\theta, \phi)\sigma_0 \eta_\Omega B_L(\theta', \phi') B_{T2}(\theta, \phi)\eta_j, \tag{12}$$

where η_j is the proportion of the backscattered intensity coinciding with the jth sampling interval:

$$\eta_j = \frac{1}{\Delta t}\left|\left[\frac{2r}{c}, \frac{2r}{c} + \Delta t\right) \bigcap [(j-1)\Delta t, j\Delta t)\right|$$

$$= \begin{cases} 1 - \left|\dfrac{r}{\Delta r} - (j-1)\right| & \text{if } (j-2)\Delta r \leq r < j\Delta r \\ 0 & \text{otherwise,} \end{cases} \tag{13}$$

where $\Delta r = c\Delta t/2$ is the range resolution.

2. Multi-beam observations of multiple targets

Now consider the more general scenario of multiple targets detected in multiple beams. Invoke the assumption of

linearity[41,42] and treat the processes of emission and reception separately. For each target l, the total incident intensity $I_{\mathrm{inc},l,f}$, at frequency f, is the sum $\sum_{i:f_i=f} I_{\mathrm{inc},i,l}$ of the incident intensities from all transmitted beams of equal frequency $f_i = f$. The intensity $I_{\mathrm{rec},j,i,l}$ received from target l in sampling interval j of beam i is calculated by

$$I_{\mathrm{rec},j,i,l} = I_{\mathrm{inc},l,f_i}\sigma_0\eta_\Omega B_{\mathrm{L}}(\theta',\phi')B_{\mathrm{T2}}(\theta,\phi)\eta_j. \tag{14}$$

The expected received intensity in sampling interval j of beam i is given by the sum $I_{\mathrm{rec},j,i} = \sum_l (I_{\mathrm{rec},j,i,l})$ of the intensities received from all targets for which $\eta_j > 0$.

In the simulation model, the randomness due to constructive and destructive interference is added either by considering $I_{\mathrm{rec},j,i}$ to be the mean of an exponentially distributed variable (originating from the Rayleigh approximation, see Sec. I D) or by applying $\beta_n = \sqrt{I_{\mathrm{rec},j,i}}$ in the PDF of the intensity from a finite number of scatterers, calculated by Barakat[31] (his Eqs. 31 and 64), depending on a measure of the number of significant scatterers

$$n_{j,i} = \sum_l \sqrt{I_{\mathrm{rec},j,i,l}} \Big/ \max_l(\sqrt{I_{\mathrm{rec},j,i,l}}). \tag{15}$$

The exact but computationally intensive PDF given by Barakat[31] is only used when $n_{j,i}$ is smaller than a user specified value.

To interpret multi-beam sonar data as a three-dimensional (3-D) image, a system of disjoint volume elements (voxels) is defined so that, simultaneously, the overlap between neighboring voxels is minimized, and the voxel volume is chosen according to the equivalent beam angle ψ. For single circular beams, the voxels are defined similarly to the volume V in Eq. (8) by the enclosure of the conical surface $\phi = \arccos(1 - \psi/2\pi)$, and the spherical surfaces $\eta_j = 1/2$. This results in voxels shaped like curved discs of constant thickness Δr and linearly increasing radius along the beam.

When multiple beams are considered, with equally separated maximum responses in both the horizontal and vertical direction, the angular partitioning is specified by surfaces of constant azimuth angle $\theta^\star$ and elevation angle $\phi^\star$ in the spherical coordinate system of the vessel (Sec. II A 1), in such a way that these angles fall in the middle between neighboring beam maxima. The resulting voxels are shaped like curved rectangular boxes with constant thickness Δr and linearly increasing angular size along the beams.

3. Measurement calibration

To make accurate acoustic measurements of fish, it is essential to calibrate the instrument.[43] This is generally accomplished by comparing theoretical and measured TS of a standard sphere. To compare theoretical and simulated TS, values of B_{T1}, B_{T2}, and α are input to Eq. (12), and I_0 is estimated for the echo from a spherical, incompressible target (i.e., a simulated standard sphere) located on the acoustic axis of each beam. The range dependent amplification $10^{\alpha r_j/5} r_j^4$, commonly known as time varied gain[44] or TVG is applied for the distance $r_j = (j-1)\Delta r$ to the jth voxel.

To compare theoretical and simulated volume backscattering coefficient s_v, a large number of uniformly distributed spherical targets are positioned in a spherical shell extending well beyond the specified sampling volume. Because of the constant range resolution, the volume of a voxel is proportional to r^2, and the volume V in Eq. (6) can be replaced by a constant times r^2, resulting in the TVG expression $10^{\alpha r_j/5} r_j^2$. For a multi-beam system, the targets contribute to the I_{rec} of all beams of equal frequency, so the beams cannot be calibrated separately.

C. Materials

Three echosounders and sonars were implemented in the simulation model: The EK60 multi-frequency echosounder, the ME70 multi-beam echosounder, and the MS70 multi-beam sonar. The simulation model was configured for the three systems according to the settings stored in real data.

1. Survey data

Data of herring from the EK60 and the MS70, collected on RV "G.O. Sars" in the Norwegian Sea outside of Tromsø, during November 2009, were used for the configuration of the simulation model, the design of the simulation experiments, and the interpretation of the simulation results for these two systems. Calibration data from the MS70, recorded on RV "G.O. Sars" on 17 December 2008 in a fjord close to Bergen, Norway, using the method described by Ona *et al.*,[45] made the basis for simulated calibration data. ME70-data of sand eel were collected on the vessel "Simrad Echo" late April 2010 in the North Sea outside the southernmost point of Norway and were used to configure the simulation model for the ME70 multi-beam echosounder.

2. EK60

The EK60 system was operated at the six frequencies 18, 38, 70, 120, 200, and 333 kHz. All of the transducer beams were virtually circularly symmetrical and pointing vertically downwards. Two-way beam widths were approximately 7.7° (10.9° one-way) for the lowest frequency and decreasing from 4.9° to 4.6° (7.0° to 6.4° one-way) with increasing frequency for the other beams. The duration of the sampling intervals was 2.56^{-4} s, giving a resolution along beams ≈ 19 cm. From the lowest to the highest frequency, measurements spanned a few thousand to a couple hundred meters.

In the simulation model, the beam patterns of the EK60 were modeled by a circular piston

$$B_{\mathrm{CP}}(\phi;k,a) = \left(\frac{2J_1(ka\sin(\phi))}{ka\sin(\phi)}\right)^2, \tag{16}$$

where a is the radius of the circular piston, ϕ is the elevation angle in the spherical coordinate system of the transducer (Sec. II A 1), and J_1 is the first order Bessel function of the first kind. Identical beam patterns were used for emission and reception, resulting in side lobe levels measuring −35.1

dB. The circular piston model was fitted to the beam widths reported in the real data.

3. ME70

The ME70 was configured with one fan of 15 beams projecting downward with an athwartship swath of approximately 60°. The frequencies of these beams ranged from 75 for the central beam aiming vertically downward to 115 and 112 kHz for the outermost beam on the port and starboard sides, respectively. The beams were non-circular and frequency dependent with two-way beam widths ranging from 2.3° to 3.5° (3.2° to 5.0° one-way) alongship and from 2.6° to 3.5° (3.7° to 4.9° one-way) athwartship. Higher frequencies, and therefore small beam angles, were used for the outer beams. Additionally, the ME70 was configured with two split-aperture reference beams at the frequencies 70 and 120 kHz, having two-way beam widths of 4.8° (6.8° one-way). Side lobe levels were between −35 and −70 dB, depending on beam width and frequency configuration. For all of the beams, the duration of the sampling intervals was 1.28^{-4} s, resulting in a resolution along beams ≈9 cm. Data collection range was set to 200 m for all beams.

In the simulation model, the non-circular beam patterns were modeled as those from a circular piston with radius $a(\theta)$ varying as an elliptical function of azimuth angle θ in the spherical coordinate system of the transceiver. In addition, the beam patterns were raised to a power of $\zeta(\theta)$, also given as an elliptical function of θ, resulting in the following expression for the non-circular beam patterns:

$$B_{\mathrm{T1}}(\theta,\phi;k,a,\zeta) = B_{\mathrm{CP}}(\phi;k,a(\theta))^{\zeta(\theta)}, \tag{17}$$

where the parameters of the elliptical functions $a(\theta)$ and $\zeta(\theta)$ were estimated based on the beam widths and side lobe levels, respectively, specified in the real data. Identical beam patterns were used for emission and reception.

4. MS70

The MS70 was configured in "continuous-wave" mode. Its 500 beams were set to comprise 20 fans, each operating at different frequencies and spanning 60° horizontally, ensonifying a volume with dimensions of 60° horizontally and 45° vertically. Each transmission sequence was set to begin with the four lowest fans, where the lowest fan operated at 112 kHz, aiming 45° downward relative to the surface and continuing with the next four fans until the last fan, operating at 75 kHz, aiming 0° relative to the surface. The two-way beam widths varied from 4.5° to 5.1° (6.4° to 7.2° one-way) vertically and from 2.7° to 4.6° (3.8° to 6.5° one-way) horizontally. With a constant frequency within each horizontal fan, the sidelobe levels were −25 dB horizontally and −35 dB vertically. The duration of the sampling intervals was 5.12^{-4} s, giving a resolution along beams ≈38 cm. Data collection range was set to 500 m in the data from November 2009 and 30 m in the calibration data from December 2008.

The non-circular beam pattern model described in the preceding text for the ME70 was used for the MS70 as well, fitted to the beam widths and side lobe levels specified in the real data.

III. SIMULATION SETUP AND RESULTS

To illustrate the use of the simulation model, five simulation experiments were conducted; one for a multi-frequency EK60, one for an ME70, and three for an MS70. This section presents these experiments and in particular describes the methods used to compare simulated MBS data to measurements of a standard sphere and of fish schools made with an MS70 aboard RV "G.O. Sars."

A. EK60 simulation

A transect of 100 transmissions was simulated across a fish school with an initial ellipsoidal shape with axes equal to 35, 35, and 20 m in the x, y, and z directions, respectively, centered at depth $d = 175$ m. The school contained approximately 5×10^5 fish and had a density equal to five fish per cubic meter.[46] The center of the school moved east at 0.6 m/s, and the vessel moved southeast at 5.2 kn. The $\mathbf{v}$ in Eq. (11) was $(0.2, 0.2, 0.2)^2$, which, for the given school speed, resulted in polarization $p = 16.9°$ (Sec. II A 4). The time between simulated transmissions was 0.67 s. In Fig. 2(a), each transmission is plotted as a vertical line of pixels, and all 100 transmissions are plotted for each frequency.

The simulated data were compared to the echogram of a herring school observed with an EK60 aboard RV "G.O. Sars" on 17 November 2009, 08:35:05 to 08:36:40 UTC [Fig. 2(b)]. The time between transmissions in the real data was 1.625 s, resulting in fewer observations across the school and apparently narrower horizontal school extent for the real data [Fig. 2(b)] compared to the simulated data [Fig. 2(a)]. Because the beam width is larger at the lower frequency, the echogram is subject to a higher degree of smearing along the time axis at this frequency, visible both in the simulated and real echograms.

There is a discrepancy between the simulated and the real echogram for the highest frequency. A possible explanation for this may be that the directionality in the backscatter from individual herring is stronger at this frequency compared to the lower frequencies. As a consequence, the total backscatter from the school is more sensitive to mean swim bladder orientation at the highest frequency.

Multiple scattering inside sufficiently dense schools results in weaker, delayed echoes.[47] This effect is apparent in the EK60 echograms as smearing of the real school toward the seabed [Fig. 2(b)]. Sound extinction due to scattering and absorption within the targets[48] will also reduce the intensity of the transmitted signal as it propagates through the school. Therefore the simulated data could be more realistic if account was made for multiple scattering or absorption within the school.

B. ME70 simulation

The same fish trajectories and the same vessel positions that were used in the simulated EK60 transect were also applied to the ME70 simulations. By overlaying echo data

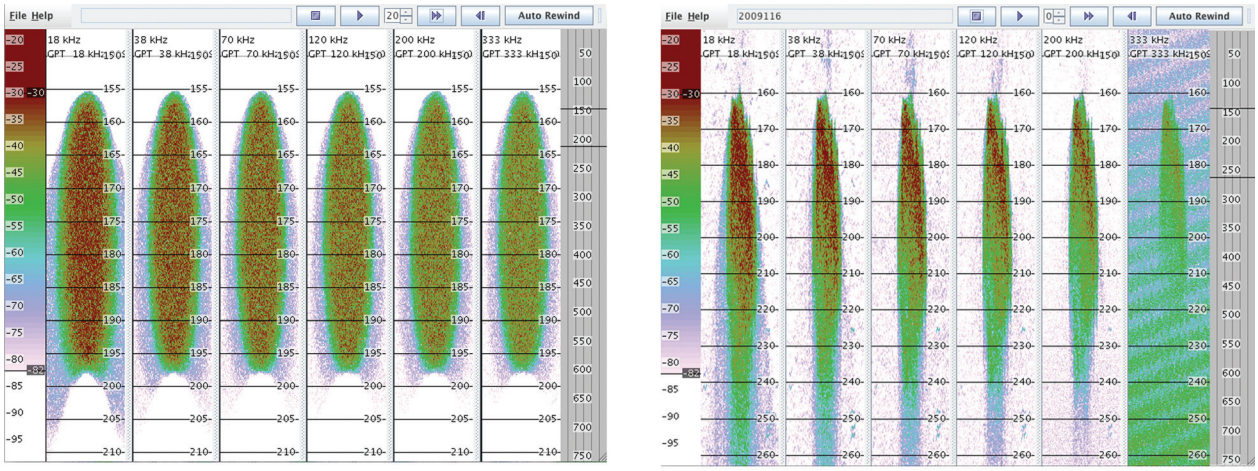

FIG. 2. (a) Simulated EK60 echogram of a school of approximately 5×10^5 fish with frequency dependent maximum backscattering cross sectional area $\sigma_0(f) = \epsilon_\sigma(f)S^2$, where $\epsilon_\sigma(f) = 10^{-6.54}(f/f_0)^{-0.4}$ and the reference frequency is $f_0 = 38$ kHz (Sec. II A 3). (b) Real EK60 echogram of a school of herring recorded on RV "G. O. Sars," 17 November 2009 (08:35:05 to 08:36:40 UTC). The real data are not corrected for ambient noise, which is high at 333 kHz.

from consecutive transmissions, a 3-D representation of the school was constructed (Fig. 3). The simulated ME70 transect illustrates the potential effect of school motion on aggregated 3-D rendering of the ME70 data. For the given velocities of the school (0.6 m/s east) and the vessel (5.2 kn southeast), the school, which is circular as seen from above, is elongated in the simulated data in the east-southeast direction (Fig. 3). As the school moves during the observation period, each slice of the school is displaced relative to the first slice by the product of school velocity and time elapsed from the first slice. For school velocities with a positive component along the vessel direction, the perceived school shape is stretched along a direction in between the directions of the vessel and the school. Conversely, for school velocities with a negative component along the vessel direction, the perceived school shape is compressed.

C. MS70 simulation

1. MS70 calibration

Special care was taken to validate the MS70 simulations. Calibration data collected on RV "G.O. Sars" on 17 December 2008 were compared to simulated calibration data, which were based on the theoretical TS values of the calibration sphere,[45,49] and positions of the calibration sphere stored in the raw files. Omnidirectional scattering directivity was applied to the calibration sphere in the simulations.

A comparison between the simulated and real calibration data for a specific transmission is shown in Fig. 4, where both color and size of the voxels indicate S_v values. The simulated calibration transmission [Fig. 4(a)] resembles the real calibration transmission [Fig. 4(b)] both in magnitude and distribution across the beams. Because targets are located to single points in the simulation model, the echo will only be shared between two consecutive sampling intervals, while the scattering from a real calibration sphere appear to be spread over at least four consecutive sampling intervals, seen as a higher number of voxels along the beams in Fig. 4(b) compared to Fig. 4(a).

2. MS70 observations of fish orientation

The second MS70 simulation experiment examined the effects of fine-scale fish-orientation patterns on measurements of s_v: Echograms were simulated for a school subject to eight different orientation scenarios [Fig. 5(a)]. The orientation scenarios involved a 90° counter-clockwise turn of the fish in vertically separated segments such as the rear half of

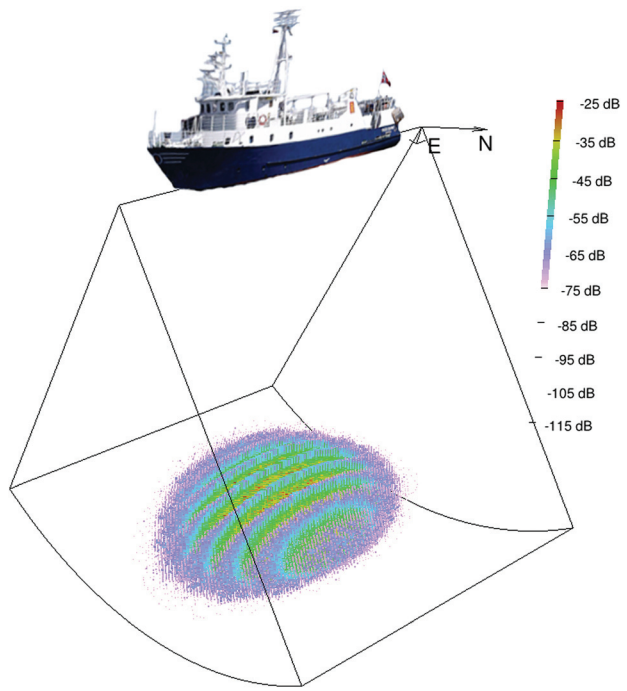

FIG. 3. Simulated ME70 echogram of a school of approximately 5×10^5 fish distributed in an ellipsoid with dimensions of 35, 35, and 20 m in the x, y, and z directions, respectively. The center of the school moved east at 0.6 m/s, and the vessel moved southeast at 5.2 kn. Each voxel is plotted as a dot with size and color representing volume backscattering strength (S_v; dB re 1 m^{-1}).

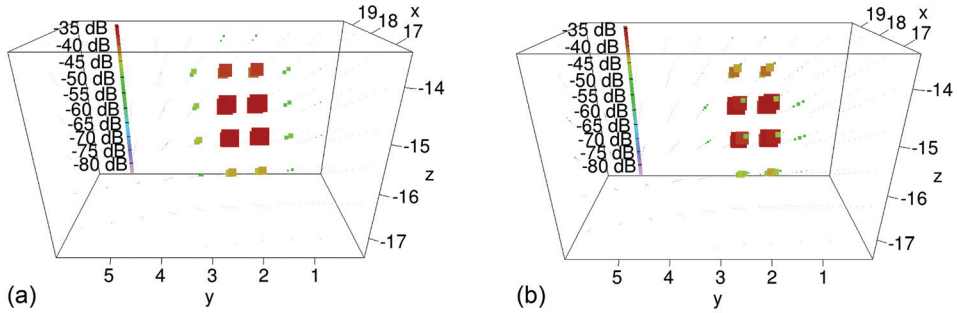

FIG. 4. Comparison of simulated (a) and real (b) data from an MS70 calibration. The real data were recorded on RV "G. O. Sars" on 17 December 2008 (22:06:19 UTC). The axes are distances (m) from the vessel position of a reference transmission. Each voxel is plotted as a dot with size and color representing volume backscattering strength (S_v; dB re 1 m^{-1}). Clusters of dots correspond to voxels along beams.

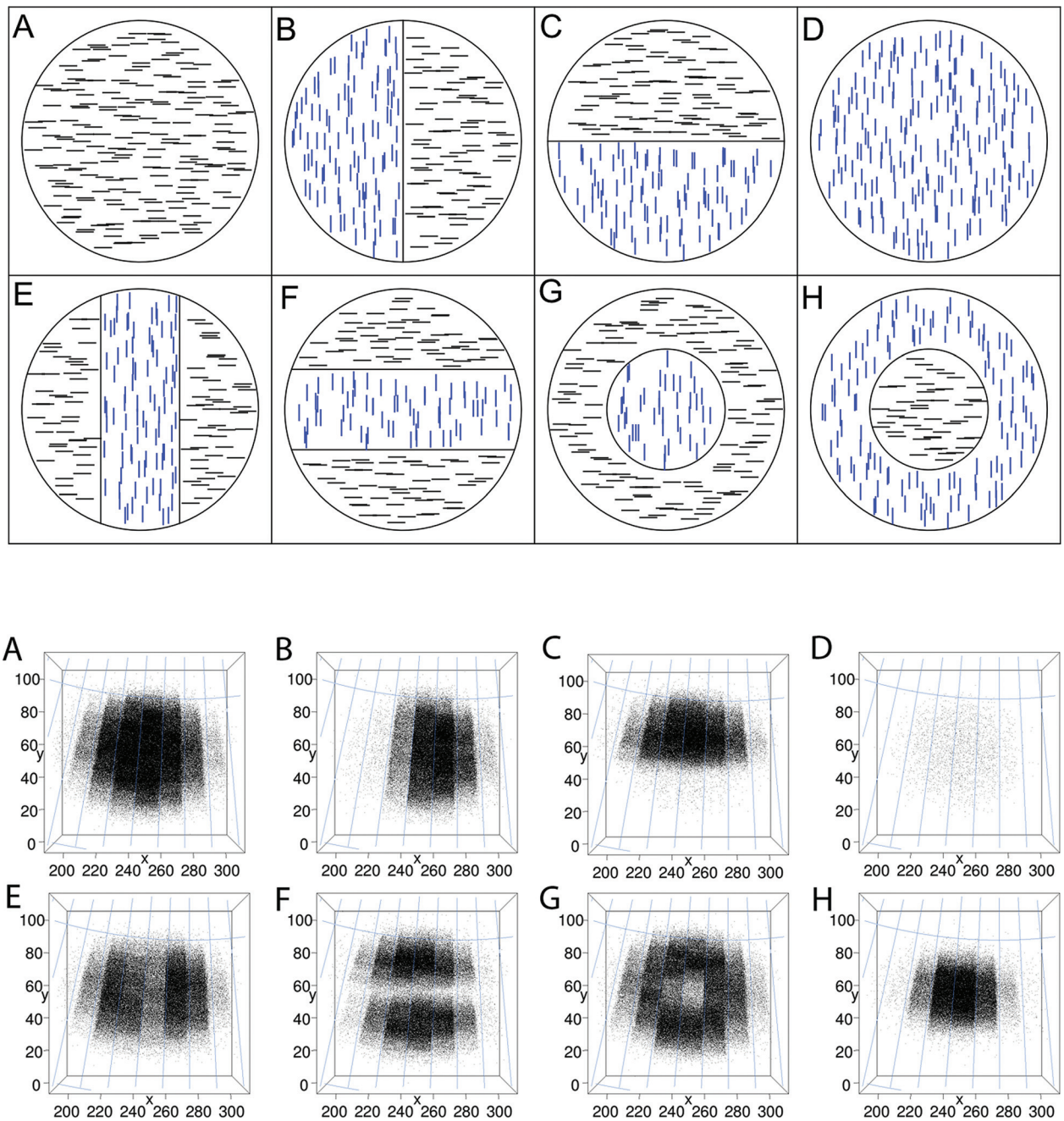

FIG. 5. (a) Top view of a graphical representation of the eight orientation scenarios applied to the school simulated in Sec. III C 2. Black lines represent fish heading east and blue lines represent fish heading north (towards the vessel). (b) Top view of 3-D point representations of the eight simulated transmissions of orientation scenarios in (a). Points are plotted uniformly in each voxel, and each point corresponds to $TS = -40$ dB. The axes are distances (m) relative to a reference vessel position.

the school [Fig. 5(a), Frame B] or a cylinder through the mass center of the school [Fig. 5(a), Frame G], serving as idealized representations of realistic schooling fish behaviors. Predator induced waves in fish orientations, starting from the edge or from the interior of the school, could potentially result in similar orientation patterns. The orientation scenarios were applied to the same school used as input to the first transmission of the simulated EK60 and ME70 transects, and the vessel was positioned 300 m north of the school. A 3-D point representation of the simulations of the orientation scenarios is shown in Fig. 5(b), where the number of uniformly distributed points plotted in each voxel is proportional to the product of s_v and volume of the voxel.

Perhaps the most striking feature of the experiment is the large drop in the simulated echo when all of the fish are oriented aligned with versus perpendicular to the sonar beams caused by the directionality of the prolate spheroidal scattering model. This effect is seen in Fig. 5(b), where the total backscatter of the school in Frame A was calculated to be 157 times higher than the total backscatter of the school in Frame D (both with polarization $p = 16.9°$). Consequently, the orientation scenarios are clearly visible in the simulations. Localized changes in fish orientations cause the school to appear as two schools in close proximity [Fig. 5(b), Frame F], or as one school with a vacuole [Fig. 5(b), Frame G]. The simulations also indicate higher along-beam versus across-beam resolutions, causing the apparent splitting of the school to be less evident in Fig. 5(b), Frame E versus Frame F.

Given that the acoustic model and degree of polarization are representative of a real school, there is also a potential for using simulations of MS70 data to infer fish density. Comparing the first transmission of the simulations of orientation scenarios to one transmission of a school of herring recorded on RV "G.O. Sars" on 13 November 2009, 13:59:25 UTC (Fig. 6), it appears that the density used in the simulations (5 fish per cubic meter) underestimates the real fish density. The mean backscatter inside a 15-m-radius sphere fully covered by the real school was more than twice the mean backscatter of the simulated school, measured inside a sphere of the same size, suggesting a packing density exceeding 10 fish per cubic meter (corresponding to 0.46 cubic meters per fish). The transmission of the real school was selected by circling around the school and choosing the transmission of highest echo. The density estimate is based on the assumptions that the distributions of fish size and orientation are similar for the real and simulated school, and that the acoustic model of the fish is sufficiently accurate.

3. MS70 observations of fish polarization

The final MS70 simulation experiment examined the polarization of a school of herring recorded during the cruise on RV "G.O. Sars" on 16 November 2009 (07:55:54 to 08:38:15 UTC). The school was located close to the surface and measured approximately 50 m across. It was observed for more than 42 min during four full circumnavigations of the school at an approximate distance of 300 m. The backscatter was highly dependent on the incidence angle (Fig. 7), which compared to the directionality of herring suggested a certain degree of polarization. By simulating the echo at all aspects, from schools of different polarizations, and comparing the total echo of the simulated and real schools, inference was made about the polarization of the real school, as shown in this section. The total backscattered energy was calculated as the sum of the product of s_v and volume of the voxels enclosed in a sphere of radius 70 m centered at the center of mass of the school for each time step. The center of mass was estimated visually, but for extended time intervals the echo from the real school was hardly distinguishable from the background noise, and the estimated centers of mass had to be interpolated between the time steps where the school was clearly visible.

The simulations were based on a school of 13 000 fish, distributed in an ellipsoid of axes 25, 25, and 10 m in the x, y, and z directions, respectively, centered at $d = 40$ m. The shape, size, and depth of the school was chosen to resemble the real school, and fish density was as low as 0.5 fish per cubic meter to make the simulations less computationally intensive. The school center was set to move at speed 0.3 m/s eastward. Five different polarizations $P = 55.1°$, $33.3°$, $16.9°$, $8.5°$, and $4.2°$ were applied to the simulated school, resulting from the five values $\mathbf{v} = (0.4^2, 0.4^2, 0.4^2)$, $(0.2^2, 0.2^2, 0.2^2)$, $(0.1^2, 0.1^2, 0.1^2)$, $(0.05^2, 0.05^2, 0.05^2)$, $(0.025^2, 0.025^2, 0.025^2)$ of the variance vector in the autoregressive

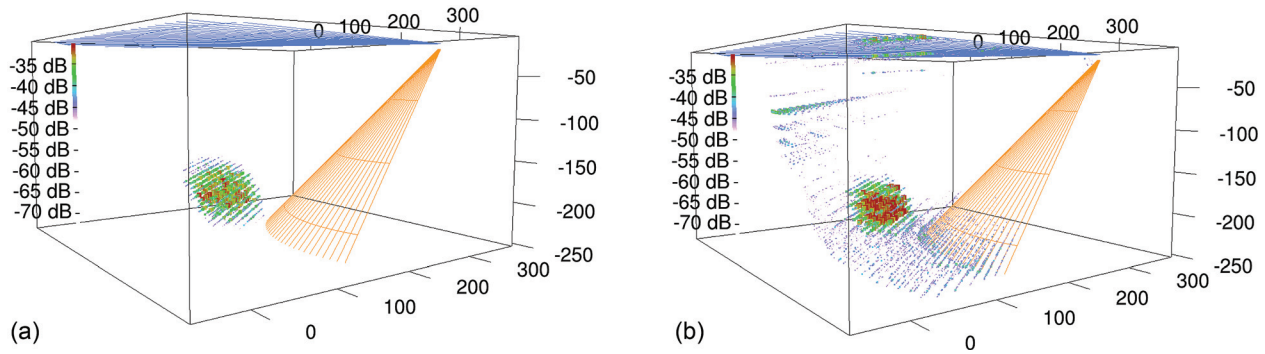

FIG. 6. (a) A simulated MS70 3-D echogram of a herring school showing the first of eight orientation scenarios simulated in Sec. III C 2. (b) A 3-D echogram of a herring school recorded with an MS70 on RV "G. O. Sars," 13 November 2009 (13:59:25 UTC). The sonar sampling volume (orange) and the surface (blue) are indicated. The axes are distances (m) relative to a reference vessel position. Each voxel is plotted as a dot with size and color representing volume backscattering strength (S_v; dB re 1 m^{-1}).

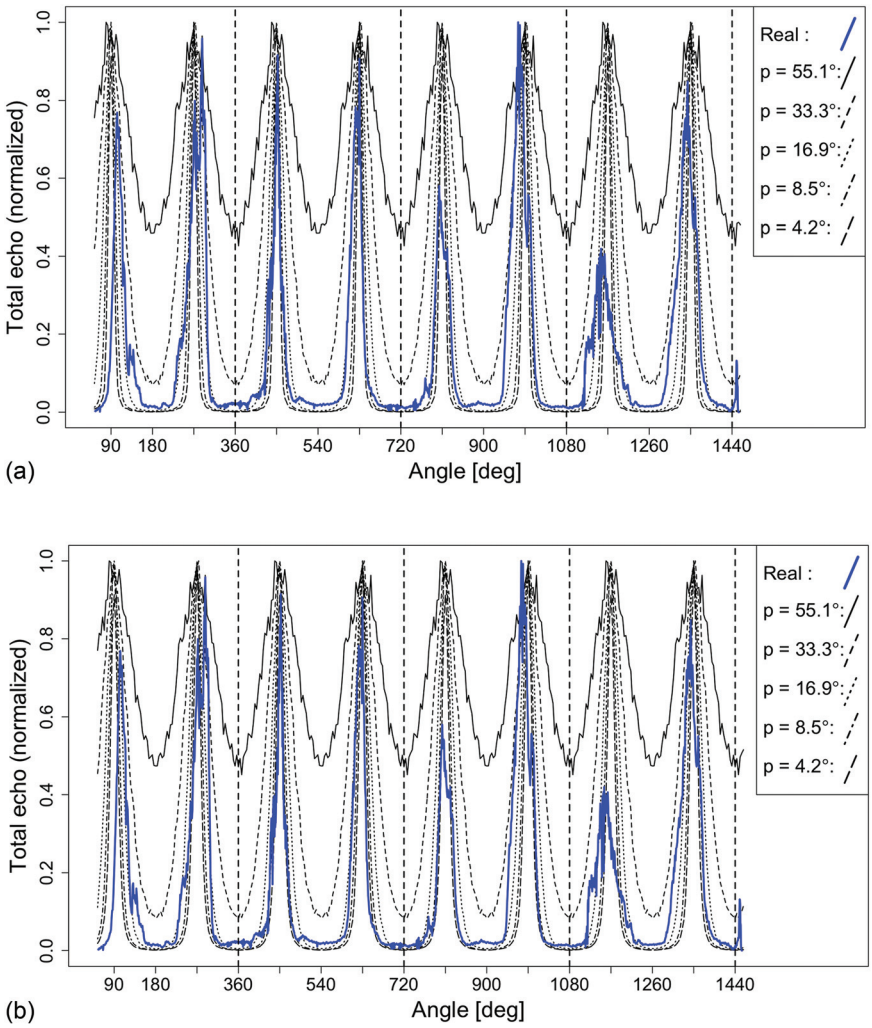

FIG. 7. Total backscatter from a near surface herring school moving south at ≈ 0.6 m/s, observed during four circumnavigations by RV "G. O. Sars," 16 November 2009 (07:55:54 to 08:38:15 UTC) and corresponding simulated data with different school polarizations (p) for (a) the line source, and (b) a prolate spheroid both with oblongness $\xi = 5$. The total backscatter from the real school (blue) and that from the simulated schools (black) is plotted versus incidence angle relative to the real school. All data are normalized, and the data of the real schools is shifted along the x axis to coincide with the real data. Full circles are indicated by vertical dotted lines.

behavior model, for the given school speed. For each polarization, the vessel positions were chosen to make one circumnavigation of 100 transmissions around the school at a distance of 300 m from the school center. The experiment was repeated for two different models of the directional factor $\eta_\Omega B_L(\theta', \phi')$ of the fish; one for the line source and one for the vacant prolate spheroid. Oblongness was 5 in all cases. The real and simulated total backscattered energy, normalized to have a maximum equal to 1, are plotted in Fig. 7. Because of differing directions of the real and simulated schools, the real data were shifted along the first axis so that the peaks of the real and simulated total backscatter values coincide.

To estimate which of the polarizations provided the closest fit to the real school, the width of the peaks in the normalized total backscatter was used. These peaks presumably occurred as the school was observed at side aspect, where the modeled backscatter from an individual target is at its maximum. For simplicity, only the fifth peak was examined, which for the line source [Fig. 7(a)] seemed to have a width somewhere between the lines for polarization $p = 16.9°$ and $p = 8.5°$. The corresponding argument for the prolate spheroid with oblongness 5 [Fig. 7(b)] seemed to favor $p \approx 8.5°$. Given the size of the school (50 m across), these polarization estimates imply a high degree of alignment, assuming that the scattering model is adequate. At the seventh peak, possible inner dynamics in the school cause the narrow orientation distribution to spread, reducing the total backscatter during this revolution.

During the cruise on RV "G.O. Sars" in November 2009, the school represented by the total echo in Fig. 7 exhibited the highest degree of polarization. Two other examples are shown in Fig. 8, plotted along with the simulated total backscatter of the prolate spheroid used in Fig. 7(b). In the upper panel, a school located close to the surface, recorded on 14 November 2009 (21:27:49 to 22:28:01 UTC), appears to be less polarized, although still showing periodic peaks indicating a common heading of the individuals. The corresponding visual analysis would place the total echo somewhere between the lines of the two least polarized simulated schools, indicating $p \in (33.3°, 55.1°)$. At the end of the observation period, the school seemed to increase its alignment after a disturbance in the periodicity of the total backscatter, possibly due to an internal or external stimuli.

In Fig. 8(b), the total backscatter of a school observed on 17 November 2009 (07:17:17 to 08:00:11 UTC) does not conform to expectations for a school of a constant direction and measurable polarization. A possible explanation for this

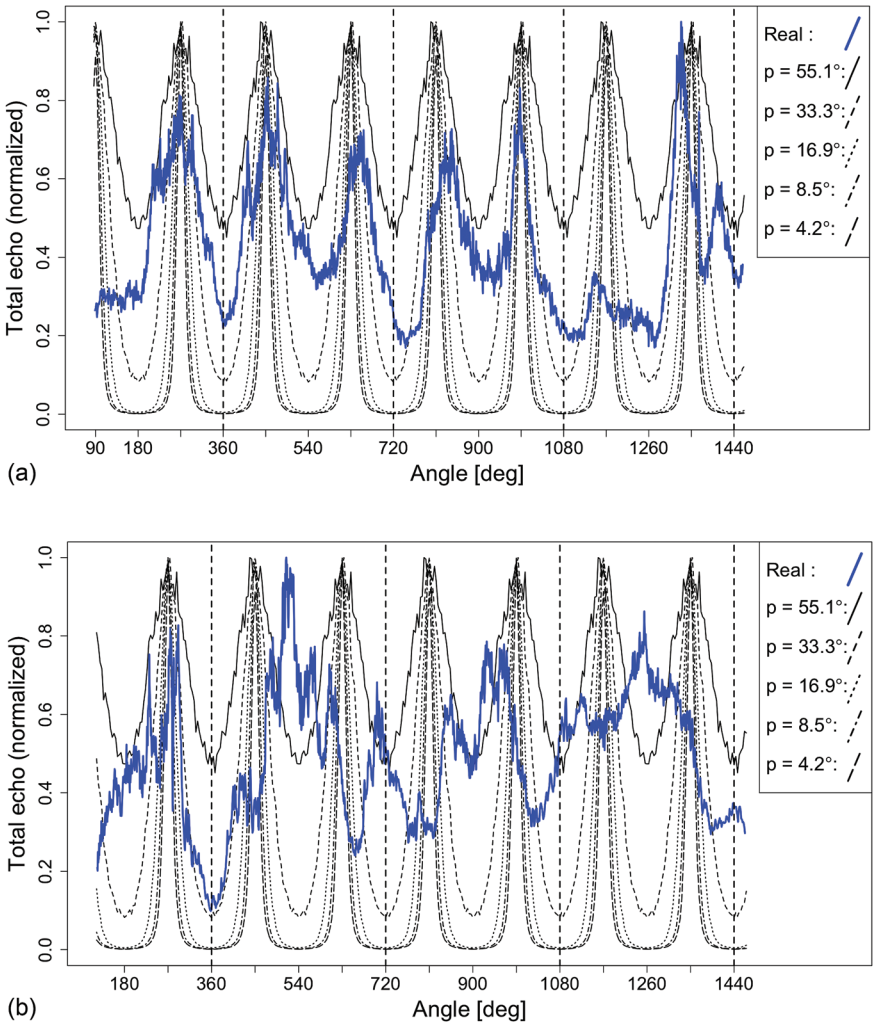

FIG. 8. Comparison between total backscatter from two schools of herring recorded on RV "G. O. Sars" on 14 November 2009 (21:27:49 to 22:28:01 UTC, school moving north-northwest at ≈0.2 m/s) and 17 November 2009 (07:17:17 to 08:00:11 UTC, school moving northeast at ≈0.45 m/s), and corresponding simulated data with different polarizations (p) for the prolate spheroid with oblongness $\xi = 5$. The total backscatter from the real school (blue) and that from the simulated schools (black) is plotted versus incidence angle. All data are normalized, and the data from the real schools are shifted along the first axis to coincide with the real data. Full circles are indicated by vertical dotted lines.

could be that the school was in a state of torus or swarming.[32] However, the total echo exhibits large and rapid fluctuations indicating a certain alignment, and the lack of a clear homogenous polarization is more likely the result of a series of observed killer whale attacks on the school during the observation period.

An alternative method for estimating the polarization could have been to quantify the relative difference in the total echo between the top of the peaks and the low regions between the peaks in Figs. 7 and 8. This method would be more robust to changes in the mean heading or to inner dynamics of schools as may be the case for the school in Fig. 8(b). However, judging from Fig. 7, the background noise could pose a problem to such a method. In the regions between peaks, the total echo of the real school generally exceeds the total echo of the simulated schools with polarizations $p \leq 16.9°$, which suggests that background noise dominates the total echo of the real school at those aspects.

IV. DISCUSSION

Three-dimensional acoustic imaging by multi-beam sonars (e.g., Simrad MS70) has introduced new possibilities for studying the morphology and dynamics of fish schools. The MS70 can record 3-D images with each transmission, enabling behavior analysis and biomass estimates of fish schools well over 100 m in size at a resolution that has not been previously available. In this work, we have shown through simulation that orientation has a profound effect on the apparent structure of fish schools recorded by the MS70 sonar. A school appearing as a vacuole or deformed in some other way, or even as two schools close by [Fig. 5(b)], can result from orientation differences between segments of the school. The simulated, aggregated 3-D image from the ME70 also demonstrated a potential disagreement between observed and actual school shape. These results encourage the use of caution when inferring spatial distributions of fish from sonar data.

Consideration of noise will result in more realistic simulation experiments than the one presented in Fig. 5. To do so, it is important to study the background noise present in real data. The potentially large effect of scattering directivity on the observed backscatter [Fig. 5(b)] emphasizes the importance of considering background noise when interpreting echoes from schools with inner dynamics or high polarization. For example, in the regions between peaks in Fig. 7, where the total echo from the real school exceeds the total echo from the simulated schools with polarization $p \leq 16.9$, the background noise may dominate the real data. For simulations based on behavior models, implementation of noise

should provide insight to the detectability of typical behavioral patterns present in real data, such as predator avoidance maneuvers[6] and spontaneous state changes,[32] making it an important consideration alongside the effect of orientation when inferring behavior from real data. When simulating echograms of targets close to the surface or seabed, it may also be necessary to include modeled reverberation from the surface and seabed, respectively, as well as refraction of the sound rays resulting from non-constant vertical sound speed profile.

Estimation of total backscatter or spatial characteristics like shape and size of schools require segmentation of the voxels associated to the school. Segmentation algorithms typically "grow" the school from an internal starting point by propagating outward and detecting the edge of the school at the voxels that no longer fulfill a criterion based on the starting point.[50] Considering the potentially dominating effect of orientation demonstrated in this paper, a criterion based on similarity to the starting point can be sensitive to within-school fish behavior. Another obstacle for segmentation is the spatial smearing of the acoustic signal due to beam width[23] and side lobe level and the shared echo between consecutive sampling intervals specified in Eq. (13). In multi-beam instruments, neighboring beams will partially overlap, and the extent depends on the beam configuration. For example, the echo from a small calibration sphere may be detected in several MS70 beams (Fig. 4). As a result, a voxel just outside of a sharp edged school may be identified as part of the school. Given that the individual positions are known in the simulation model, data simulated from a variety of school shapes and orientation structures can be used to test the performance of segmentation algorithms. This may include fragmented boundaries with the potential of adding difficulties to distinguishing between noise and fish at these boundaries.

One simulation experiment (Fig. 5) demonstrated the large potential error involved in estimating biomass from multi-beam sonar echoes. The simulated total backscatter from a school at depth $d = 175$ m and with polarization $p = 16.9°$, where the swim bladder was modeled by a vacant prolate spheroid with oblongness $\xi = 5$, and scattering from the rest of the fish body was ignored, was 157 times higher when mean heading of the fish was perpendicular to versus aligned with the sonar beams [Fig. 5(b), Frames 1 and 4]. Large changes in backscatter due to changes in orientation are also observed in real data (e.g., Figs. 7 and 8). Consequently, the sampling design for surveys of migrating fish may bias (horizontally) acoustically estimated biomass. In other words, if a vessel transits a sampling grid and the fish schools are polarized and migrating in a particular direction, the acoustic incidence angles will not be random and the echo energy will be affected. This potential bias may be estimated using the simulation model. For a given survey design, correction factors may be estimated by generating acoustic backscatter data for schools with various densities, polarizations, and mean headings and comparing it to theory.

As shown in this study, the results of simulations of acoustic data can be used to improve estimates of biomass and interpretations of acoustic data with respect to behavior, requiring that the acoustic scattering from targets as well as the intensity perceived by real instruments are accurately modeled. In most of the simulations, the PSMS model[15] (supplemented by the KRM model for the highest frequencies) was used to calculate the scattering directivity of the targets. However, in the experiment illustrated in Fig. 7, the polarization of a real school was estimated based on simulations using the PSMS model [$p \in (8.5°, 16.9°)$] and the line source model ($p \approx 8.5°$), showing that the choice of scattering model for the targets may affect the interpretation of the data based on simulations. Repeating the simulations using more sophisticated models (e.g., Reeder *et al.*[18]) and measurements of backscattering directivity (Pedersen *et al.*[11]), could identify the sensitivity of the interpretation of acoustic data with respect to the choice of scattering model.

The on-axis TS applied to the simulations based on Ona[39] involved the maximum backscattering cross-section $\sigma_0(f0) = 10^{-6.54}S^2$ and the hydrostatic swim bladder compression $\eta_C = (1 - d/10)^{-0.23}$. Parameters used in this expression have been reported with varying estimates depending on the experiment,[39,51,52] and the sensitivity of biomass estimates with respect to the parameters can be investigated using the simulation model. Frequency dependence of the on-axis backscatter was modeled by the factor $(f/f_0)^{-0.4}$, where $f_0 = 38$ kHz, but this empirical relationship underestimated the backscatter perceived by the real EK60 for the highest frequency $f = 333$ kHz (Fig. 2). A possible explanation (given in Sec. III C), is the increased directionality of herring backscatter at higher frequencies. This could make the simulated data more sensitive to fish and swim bladder orientations. Given the effect of orientation on the individual backscatter, variance in parameter estimates within and between experiments may generally be influenced by behavior,[4] a hypothesis that can be tested through simulation.

The effects of target orientation and density are convoluted (see Fig. 5), but both may affect estimates of biomass, school structure, and dynamics. Assuming that fish change orientations more rapidly than their school changes density, the high temporal resolution of the MS70 may disambiguate these effects. A method that identifies orientation changes as those exceeding what can be explained by density changes alone can be important for the interpretation of multi-beam sonar data with respect to behavior. The simulation model may be useful to identify to what extent a change in perceived backscatter could be due to plausible changes in density versus changes in orientation.

The simulation model was principally developed to predict multi-beam sonar images of fish schools having certain densities, morphological characteristics, and behaviors. The intention is to narrow the gap between models of fish behavior and acoustic observations of large schools *in situ*. School dynamics resulting from predator and vessel avoidance can be mimicked by behavior models, and the corresponding simulated data can be compared to real data exhibiting such behavior. For example, the estimated polarizations $p \approx 8.5°$ and $p \in (33.3°, 55.1°)$ of two near-surface schools [Figs. 7(b) and 8(a), respectively], where the target beam pattern was modeled by the PSMS model, indicated differences

in behavior. A third school [Fig. 8(b)] was investigated by the same method, but the total echo did not conform to the periodicity related to polarization, indicating a different type of behavior than the homogenous polarized state. In fact, this school experienced several killer whale attacks, which may have altered the heading of the school or parts of the school. Simulated acoustic data of herring schools responding to killer whale attacks, analyzed with respect to localized variations in the backscatter or to the polarization estimates from the total backscatter, could provide insight to the ability of the behavior models to predict anti-predator responses of large free swimming fish schools.

Modeling of echoes from individual fish in schools can improve interpretations of signals from modern sonar systems. It is likely that this modeling approach will be important when designing new algorithms and tools as well as assisting in the interpretation of the sonar images acquired in experiments and surveys.

AKNOWLEDGMENTS

The authors wish to acknowledge Dr. Kenneth G. Foote for valuable inputs during the writing process, Professor Iain D. Couzin and the Couzin lab for putting things in the right perspective, and Dr. David Demer for many valuable comments and suggestions after reading the paper. Thanks also to Gavin Macaulay for providing the PSMS model, and the crew on RV "G.O. Sars" for excellent maneuvering during data collection. Funding for the work was provided by the University of Bergen, the Institute of Marine Research, and Norwegian Research Council (Grant No. 204229/F20).

[1]J. S. Jaffe, "Using multi-angle scattered sound to size fish swimbladders," ICES J. Mar. Sci. **63**, 1397–1404 (2006).
[2]N. C. Makris, P. Ratilal, D. T. Symonds, S. Jagannathan, S. Lee, and R. W. Nero, "Fish population and behavior revealed by instantaneous continental shelf-scale imaging," Science **311**, 660–663 (2006).
[3]F. Gerlotto, M. Soria, and P. Fréon, "From two dimensions to three: The use of multibeam sonar for a new approach in fisheries acoustics," Can. J. Fish. Aquat. Sci. **56**, 6–12 (1999).
[4]K. G. Foote, "Effect of fish behaviour on echo energy: The need for measurements of orientation distributions," ICES J. Mar. Sci. **39**, 193–201 (1980).
[5]K. M. Boswell, B. M. Roth, and J. H. Cowan, "Simulating the effects of side-aspect fish orientation on acoustic biomass estimates," ICES J. Mar. Sci. **66**, 1398–1403 (2009).
[6]L. Nøttestad, A. Fernö, S. Mackinson, T. Pitcher, and O. A. Misund, "How whales influence herring school dynamics in a cold-front area of the Norwegian Sea," ICES J. Mar. Sci. **59**, 393–400 (2002).
[7]B. L. Partridge, "Structure and function of fish schools," Sci. Am. **246**, 114–123 (1982).
[8]R. J. Korneliussen and E. Ona, "An operational system for processing and visualizing multi-frequency acoustic data," ICES J. Mar. Sci. **59**, 293–313 (2002).
[9]R. H. Love, "Target strength of an individual fish at any aspect," J. Acoust. Soc. Am. **62**, 1397–1402 (1977).
[10]E. Ona, "Physiological factors causing natural variations in acoustic target strength of fish," J. Mar. Biol. Assoc. U.K. **70**, 107–127 (1990).
[11]G. Pedersen, N. O. Handegard, and E. Ona, "Lateral-aspect, target-strength measurements of in situ herring (*Clupea harengus*)," ICES J. Mar. Sci. **66**, 1191–1196 (2009).
[12]D. A. Demer and S. G. Conti, "New target-strength model indicates more krill in the Southern Ocean," ICES J. Mar. Sci. **62**, 25–32 (2005).
[13]K. Amakasu and M. Furusawa, "The target strength of Antarctic krill (*Euphausia superba*) measured by the split-beam method in a small tank at 70 kHz," ICES J. Mar. Sci. **63**, 36–45 (2006).
[14]S. McClatchie and Z. Ye, "Target strength of an oily deep-water fish, orange roughy (*Hoplostethus atlanticus*). II. Modeling," J. Acoust. Soc. Am. **107**, 1280–1285 (2000).
[15]Y. Tang, Y. Nishimori, and M. Furusawa, "The average three-dimensional target strength of fish by spheroid model for sonar surveys," ICES J. Mar. Sci. **66**, 1176–1183 (2009).
[16]S. McClatchie, J. Alsop, Z. Ye, and R. F. Coombs, "Consequence of swimbladder model choice and fish orientation to target strength of three New Zealand fish species," ICES J. Mar. Sci. **53**, 847–862 (1996).
[17]C. S. Clay and J. K. Horne, "Acoustic models of fish: The Atlantic cod (*Gadus morhua*)," J. Acoust. Soc. Am. **96**, 1661–1668 (1994).
[18]D. B. Reeder, J. M. Jech, and T. K. Stanton, "Broadband acoustic backscatter and high-resolution morphology of fish: Measurement and modeling," J. Acoust. Soc. Am. **116**, 747–761 (2004).
[19]K. G. Foote, "Simulating echograms," ICES J. Mar. Sci. **B**, 6 (1989).
[20]O. Dragesund and S. Olsen, "On the possibility of estimating year-class strength by measuring echo-abundance of 0-group fish," Fiskeridir. Skr., Ser. Havunder. **13**, 48–75 (1965).
[21]K. G. Foote and O. Nakken, "Dorsal aspect target strength functions of six fishes at two ultrasonic frequencies," Fisk. Havet Ser. B **3**, 1–96 (1978).
[22]R. F. Coombs and R. Barr, "Acoustic remote sensing of swimbladder orientation and species mix in the oreo population on the Chatham Rise," J. Acoust Soc. Am. **115**, 1516–1524 (2004).
[23]N. Diner, "Correction on school geometry and density: Approach based on acoustic image simulation," Aquat. Living Res. **14**, 211–222 (2001).
[24]D. A. Demer, M. A. Soule, and R. P. Hewitt, "A multiple-frequency method for potentially improving the accuracy and precision of in situ target strength measurements," J. Acoust. Soc. Am. **105**, 2359–2376 (1999).
[25]J. K. Horne and J. M. Jech, "Multi-frequency estimates of fish abundance: Constraints of rather high frequencies," ICES J. Mar. Sci. **56**, 184–199 (1999).
[26]B. Buelens, R. Williams, A. Sale, and T. Pauly, "Model inversion for midwater multibeam backscatter data analysis," in *IEEE Oceans 05 Europe*, Brest, France (2005), Vol. 1, pp. 431–435.
[27]G. R. Cutter and D. A. Demer, "Accounting for scattering directivity and fish behaviour in multibeam-echosounder surveys," ICES J. Mar. Sci. **64**, 1664–1674 (2007).
[28]M. J. Henderson, J. K. Horne, and R. H. Towler, "The influence of beam position and swimming direction on fish target strength," ICES J. Mar. Sci. **65**, 226–237 (2008).
[29]T. K. Stanton, "Volume scattering: Echo peak PDF," J. Acoust. Soc. Am. **77**, 1358–1366 (1984).
[30]D. Chu and T. Stanton, "Statistics of echoes from a directional sonar beam insonifying finite numbers of single scatterers and patches of scatterers," IEEE J. Ocean. Eng. **35**, 267–277 (2010).
[31]R. Barakat, "First-order statistics of combined random sinusoidal waves with applications to laser speckle patterns," Opt. Acta: Int. J.Opt. **21**, 903–921 (1974).
[32]I. D. Couzin, J. Krause, R. James, G. D. Ruxton, and N. R. Franks, "Collective memory and spatial sorting in animal groups," J. Theor. Biol. **218**, 1–11 (2002).
[33]J. Paramo, F. Gerlotto, and C. Oyarzun, "Three dimensional structure and morphology of pelagic fish schools," J. Appl. Ichthyol. **26**, 853–860 (2010).
[34]R. J. Korneliussen, Y. Heggelund, I. K. Eliassen, O. K. Øye, T. Knutsen, and J. Dalen, "Combining multibeam-sonar and multifrequency-echosounder data: Examples of the analysis and imaging of large euphausiid schools," ICES J. Mar. Sci. **66**, 991–997 (2009).
[35]F. Gerlotto, S. Bertrand, N. Bez, and M. Gutierrez, "Waves of agitation inside anchovy schools observed with multibeam sonar: A way to transmit information in response to predation," ICES J. Mar. Sci. **63**, 1405–1417 (2006).
[36]J. K. Parrish, S. V. Viscido, and D. Grünbaum, "Self-organized fish schools: An examination of emergent properties," Biol. Bull. **202**, 296–305 (2002).
[37]D. N. MacLennan, P. G. Fernandes, and J. Dalen, "A consistent approach to definitions and symbols in fisheries acoustics," ICES J. Mar. Sci. **59**, 365–369 (2002).
[38]E. J. Simmonds, "A comparison between measured and theoretical equivalent beam angles for seven similar transducers," J. Sound Vib. **97**, 117–128 (1984).

[39]E. Ona, "An expanded target-strength relationship for herring," ICES J. Mar. Sci. **60**, 493–499 (2003).
[40]N. Gorska and E. Ona, "Modelling the acoustic effect of swimbladder compression in herring," ICES J. Mar. Sci. **60**, 548–554 (2003).
[41]K. G. Foote, "Linearity of fisheries acoustics, with addition theorems," J. Acoust. Soc. Am. **73**, 1932–1940 (1983).
[42]D. N. MacLennan, "Acoustical measurement of fish abundance," J. Acoust. Soc. Am. **87**, 1–15 (1990).
[43]K. G. Foote, H. P. Knudsen, G. Vestnes, D. N. MacLennan, and E. J. Simmons, "Calibration of acoustic instruments for fish density estimation: A practical guide," Cooperative Research Report 144, International Council for the Exploration of the Sea (1987).
[44]D. MacLennan, "Time varied gain functions for pulsed sonars," J. Sound Vib. **110**, 511–522 (1986).
[45]E. Ona, V. Mazauric, and L. N. Andersen, "Calibration methods for two scientific multibeam systems," ICES J. Mar. Sci. **66**, 1326–1334 (2009).
[46]B. Pedersen and M. V. Trevorrow, "Continuous monitoring of fish in a shallow channel using a fixed horizontal sonar," J. Acoust. Soc. Am. **105**, 3126–3135 (1999).
[47]I. B. Andreeva and A. V. Belousov, "Multiple sound scattering by densely packed shoals of marine animals," ICES J. Mar. Sci. **53**, 323–327 (1996).
[48]K. G. Foote, "Extinction cross-section of Norwegian spring-spawning herring," ICES J. Mar. Sci. **56**, 606–612 (1999).
[49]K. Foote, "Optimizing two targets for calibrating a broadband multibeam sonar," in *OCEANS 2006*, pp. 1–4.
[50]J.-P. Balabanian, I. Viola, E. Ona, R. Patel, and E. Gröller, "Sonar explorer: A new tool for visualization of fish schools from 3D sonar data," in *Eurographics/ IEEE-VGTC Symposium on Visualization* (2007), pp. 155–162.
[51]K. G. Foote, "Fish target strengths for use in echo integrator surveys," J. Acoust. Soc. Am. **82**, 981–987 (1987).
[52]T. Didrikas and S. Hansson, "In situ target strength of the Baltic Sea herring and sprat," ICES J. Mar. Sci. **61**, 378–382 (2004).